

pubs.acs.org/JPCC Article

# Direct and Indirect DNP NMR Uncovers the Interplay of Surfactants with Their Mesoporous Host Material

Sonja C. Döller, Martin Brodrecht, Torsten Gutmann, Markus Hoffmann, and Gerd Buntkowsky\*





ACCESS

Metrics & More

Article Recommendations

Supporting Information

direct
both
both
indirect

pW off '5

140 120 100 80 80 40 20 0

**ABSTRACT:** Two different mesoporous silica materials (SBA-15 and MCM 41) were impregnated with four different, commercially available surfactants, namely,  $E_5$ , PEG 200,  $C_{10}E_6$ , and Triton X-100. Differential scanning calorimetry was employed to confirm the confinement of the surfactants in the pores of their host materials. Dynamic nuclear polarization enhanced solid state  $^{13}$ C magic angle spinning (MAS) nuclear magnetic resonance (NMR) spectra were recorded for these materials, showing that both the direct as well as the indirect polarization transfer pathways are active for the carbons of the polyethylene glycol moieties of the surfactants. The presence of the indirect polarization pathway implies the presence of molecular motion with correlation times faster than the inverse Larmor frequency of the observed signals. The intensities of the signals were determined, and an approach based on relative intensities was employed to ensure comparability throughout the samples. From these data, the interactions of the surfactants with the pore walls could be determined. Additionally, a model describing the surfactants' arrangement in the pores was developed. It was concluded that all carbons of the hydrophilic surfactants,  $E_5$  and PEG 200, interact with the silica walls in a similar fashion, leading to similar polarization transfer pathway patterns for all observed signals. For the amphiphilic surfactants  $C_{10}E_6$  and Triton X-100, the terminal hydroxyl group mediates the majority of the interactions with the pore walls and the polarizing agent.

# 1. INTRODUCTION

High-surface materials are of relevance for a plethora of applications such as chromatography, support materials for precious metal catalysts, adsorbents, drug-delivery systems, and many more. All of these systems rely on the interactions of a liquid phase with a solid interface. In particular, amorphous, mesoporous silica materials are of interest for industrial and academic applications since they are relatively easy to synthesize as well as due to their large surface areas and the facile functionalization of their surfaces to specific tasks. Hence, silica materials have been found to be the ideal model systems to probe surface interactions and dynamics at a molecular level. Especially the class of Santa Barbara Amorphous (SBA) and M41S phases, such as MCM 41, have been used to study confinement effects on a number of guest molecules.

Due to their non-toxicity, surfactants (surface-active agents) as well as polyethylene glycols (PEGs) play a key role in establishing green chemistry principles<sup>20,21</sup> throughout chem-

ical synthesis including catalysis<sup>22</sup> or the production of polymers<sup>23</sup> through the replacement of typical organic solvents.<sup>24</sup> Thanks to their amphiphilic nature, surfactants are able to form supramolecular aggregates. These aggregates are typically in the form of micelles in aqueous solution but may also be of other types such as lamellae, especially at high surfactant concentration or in the bulk of the neat surfactant.<sup>25–27</sup> The presence of such aggregates provides lipophilic spaces in aqueous environments where reactions can take place.<sup>24</sup>

Received: March 23, 2023 Revised: May 31, 2023 Published: June 16, 2023





Typically, the interplay of a guest molecule with a solid surface strongly alters the guest molecule's properties due to solid—liquid-interactions. These interactions are not well understood because they are generally difficult to probe at a molecular level.<sup>29</sup> Solid state nuclear magnetic resonance (ssNMR) has been established as an important tool to investigate surface chemistry and structural details, both of which further the understanding of host–guest interactions and dynamics. By utilizing  $^2\mathrm{H}$  NMR,  $^{28,30,31}$   $T_1$  measurements, 32,33 or NMR diffusometry, 34 the dynamics of systems can be uncovered in ssNMR. To overcome sensitivity issues inherent to ssNMR, dynamic nuclear polarization (DNP) is usually employed, enhancing signals by several orders of magnitude. 35-37 Recently, new methods enabling the investigation of molecular motion have been discovered by the observation of two competing polarization transfer pathways in solid state DNP NMR.<sup>38–45</sup> In the direct pathway, the polarization proceeds from the utilized polarizing agent, usually a radical or a metal ion, 46 directly to the investigated nucleus. The indirect polarization transfer pathway is facilitated by  ${}^{1}H-X$  (X =  ${}^{13}C$ ,  ${}^{15}N$ ) cross-relaxation of molecular groups due to the presence of adequate dynamics for which the nuclear Overhauser effect type of mechanism is operative. 38,40 The two pathways show opposite signs in the recorded NMR signal, leading to a superposition of two sets of resonances. This distinction allows for site-specific probing in crowded spectra like those obtained from protein samples 42,47 or RNA, 48 the investigation of protein-ligand binding, 43 or the determination of active dynamics under low-temperature DNP conditions. 41,49

In previous works,<sup>50</sup> it has been shown that DNP-enhanced ssNMR is a suitable method to probe the interactions of guest molecules with a mesoporous host materials, allowing the development of models and the description of dynamic processes inside of the pores. Therefore, the aim of this work is to apply this methodology in an attempt to understand how different classes of surfactants interact with a host material with a hydrophilic surface, namely mesoporous silica, for the purpose of developing a model of their arrangement in the pores. Additionally, the influence of pore size on the confinement is investigated to conclude whether it has a significant effect on the self-assembly of the surfactants.

In this work, the four different analyte molecules shown in Figure 1, pentaethylene glycol ( $E_5$ ), PEG 200, as well as the surfactants decylhexaglycol ( $C_{10}E_6$ ) and Triton X-100 (Triton), are confined in the pores of two mesoporous silica

**Figure 1.** Structures of the surfactants studied in this work. Except for  $E_5$ , the surfactants are polydisperse mixtures, and their exact compositions can be found in a prior report<sup>40</sup> and are collected in the Supporting Information in Table S1.

materials with different pore sizes, namely SBA-15 and MCM 41. For simplification, all analyte molecules are further referred to as surfactants. PEG 200, C<sub>10</sub>E<sub>6</sub>, and Triton are produced at an industrial scale and are used as polydisperse mixtures.<sup>40</sup>  $^{1}H \rightarrow {}^{13}C$  CP MAS ssNMR spectra are recorded to estimate an enhancement factor for each sample, employing the hydrophilic binitroxyl radical AMUPol as polarization agent.<sup>51</sup> To analyze the interactions of the surfactants with the walls of the mesopores, <sup>13</sup>C MAS DNP-enhanced ssNMR measurements are performed at different buildup times. The contribution of the direct and indirect polarization transfer pathways is analyzed for the carbons located in the PEG moiety of each surfactant. To achieve comparability for all investigated samples, an approach based on relative intensities is employed.<sup>49</sup> Finally, differential scanning calorimetry (DSC) is employed to probe the phase behavior of the different surfactants while confined in the mesoporous silica materials, which is compared to those of the AMUPol dissolved in the bulk surfactants.

#### 2. MATERIALS AND METHODS

**2.1. General.** All chemicals were used as received.  $E_5$  was purchased from Alfa Aesar. AMUPol was purchased from CortecNet. The utilized polydisperse surfactants PEG 200,  $C_{10}E_6$ , and Triton were generously donated by Rochester Midland Corporation. Further details on the mixture composition of the polydisperse surfactants were published in a prior report and are collected in the Supporting Information in Table S1. The chemicals used for the synthesis of the mesoporous silica materials were purchased from Acros, Sigma-Aldrich, Carl Roth, and ABCR. All chemicals were used without further purification unless explicitly mentioned. Details on all chemicals (including the surfactants) used in this work are shown in Table S2 in the Supporting Information.

2.2. Synthesis of the Mesoporous Silica Materials. 2.2.1. Synthesis of SBA-15. Mesoporous SBA-15 was synthesized according to the literature. 52,53 21.3 g (0.017 equiv) of Pluronic123 was dissolved in 574.0 mL (165.0 equiv) of demineralized water overnight. To this solution, 108.0 mL (6.0 equiv) of 37 wt % hydrochloric acid was added to yield a concentration of HCl of 1.9 mol L<sup>-1</sup>. The solution was heated to 40 °C and allowed to equilibrate overnight. Afterward, 47.9 g (1.0 equiv) of tetraethyl orthosilicate (TEOS) was slowly added while stirring. Stirring was continued for 1 h, resulting in a white precipitate. This suspension was stirred at 40 °C for 24 h and was then transferred into a polytetrafluoroethylene (PTFE) bottle. The bottle was stored under static conditions at 90 °C for 48 h. The obtained white precipitate was washed with demineralized water twice and with ethanol once by centrifugation. The leftover template was removed by calcination at 650 °C, yielding 11.70 g of SBA-15 mesoporous silica.

2.2.2. Synthesis of MCM 41. MCM-41 (C<sub>18</sub>) was synthesized by an optimized protocol based on a protocol reported previously.<sup>34</sup> For this, 14.2 g (36.3 mmol, 0.13 equiv) trimethyloctadecylammonium bromide (C<sub>18</sub>TAB/stearyltrimethylammonium bromide) was dissolved in 672 mL demineralized water. The mixture was heated to 35 °C. After that, 58.5 mL ammonia solution (25 wt %) was added and the solution was stirred for another 1.5 h until everything was fully dissolved. Afterward, 60.0 g (269 mmol, 1.00 equiv) TEOS was slowly added. After the addition was complete, the suspension was stirred for 1 h. This suspension was then

transferred into a PTFE bottle and aged under static conditions at 80  $^{\circ}\text{C}$  for 72 h. After ageing, the white precipitate was filtered off. The porous silica was washed with demineralized water and the leftover template was removed by calcination at 650  $^{\circ}\text{C}.$ 

**2.3.** Characterization of the Mesoporous Silica Materials. 2.3.1. Sample Preparation. The wet samples were transferred into a glass burette and predried at mild vacuum (approximately 10 mbar) over night. After predrying, the samples were dried using a turbomolecular pump  $(10^{-6} \text{ mbar})$  over night. During all drying steps, the samples were heated to 80 °C. The dried samples were directly transferred to the Brunauer–Emmett–Teller (BET) analyzer. The masses of the dried samples were used for the evaluation of the adsorption/desorption measurements.

2.3.2. Adsorption—Desorption Measurements. The porosity, pore volume, and specific surface area of the materials were characterized by nitrogen adsorption at 77 K, employing a Thermo Fisher Scientific Surfer BET analyzer using N2 gas as adsorbent. The specific surface was obtained by the BET method<sup>54</sup> analyzing the curve in the  $p/p^0$  range between 0.1 and 0.4. The pore volume was obtained by the Gurvich method, 55 the  $p/p^0$  value at 0.95 was used. Blank measurements were performed using He gas. Pore size distributions were obtained by applying the Barrett-Joyner-Halenda method,<sup>56</sup> analyzing the adsorption–desorption isotherms in the  $p/p^0$  range between 0.3 and 0.95. Pore sizes obtained by nonlocal density functional theory<sup>57</sup> (NLDFT) used a model for N<sub>2</sub> adsorption on silicon at 77 K. The model for the adsorption of nitrogen on silica surfaces with cylindrical pore geometries of the Advanced Data Processing (ADP) software (V 6.2.4) was used for evaluation. Interpretation of the results follow our previous reports.34,58

**2.4.** Sample Preparation for DNP NMR and DSC Experiments. 2 mg (2.75  $\mu$ mol) of AMUPol was dissolved into 0.183 mL of the surfactants in small plastic vials to obtain a concentration of ca. 15 mmol L<sup>-1</sup>. It was necessary to employ ultrasonication for up to 20 min to achieve complete dissolution. As it has been shown that ultrasonication might lead to degradation of the polarizing agents, <sup>59</sup> the effective AMUPol concentrations may have been lower than the nominal concentration of 15 mmol L<sup>-1</sup>.

In preparation for the impregnation with the surfactants, the utilized mesoporous silica materials SBA-15 and MCM 41 were dried utilizing a turbomolecular pump at room temperature for at least 24 h. The dried silica was then transferred into a glovebox to prevent unwanted adsorption of atmospheric water.

The surfactant solutions were then transferred into aliquots of the respective silicas to fill approximately 80% of the pore volume obtained from the adsorption—desorption measurements, and the materials were left in the glovebox overnight to allow for full absorption of the surfactant solutions. Afterward, the samples were transferred into a freezer in the glovebox to prevent any further degradation of the radicals.

**2.5. DSC Measurements.** For the measurements of the surfactants confined in the silica materials, approximately 3 mg of the respective sample was transferred into a 5 mm aluminum crucible, which was sealed with an appropriate press by Netzsch. For the pure surfactant solutions, approximately 20  $\mu$ L of the sample was used for the DSC measurements.

All DSC measurements were performed on the DSC 214 Polyma apparatus by Netzsch in dynamic mode. Liquid

nitrogen was employed as cooling agent. An empty cubicle served as reference. A heating/cooling rate of  $10~\rm K~min^{-1}$  was used in the temperature range between  $100~\rm and~300~\rm K$ .

The results and discussion of the DSC measurements are shown in Section S3 of the Supporting Information.

**2.6.** DNP-Enhanced <sup>13</sup>C Solid State NMR Spectroscopy. Approximately 10 mg of the respective sample was transferred into a 3.2 mm sapphire rotor. The rotor was sealed with a Teflon plug and closed with a ZrO<sub>2</sub> driving cap.

All DNP ssNMR measurements were conducted on a Bruker AVANCE III 400 DNP NMR spectrometer operating at 9.4 T (401.63 MHz for  $^1$ H, 100.99 MHz for  $^{13}$ C) at a MAS rate of 8 kHz. A 9.7 T Bruker gyrotron system was used to generate microwaves ( $\mu$ w) at 263 GHz frequency. The spectrometer is equipped with a 3.2 mm low temperature H/X/Y triple resonance probe that was used in  $^1$ H/ $^{13}$ C/Y triple mode throughout the measurements. Sample temperatures were nominally 112 and 122 K for data obtained without and with  $\mu$ w irradiation of the sample, respectively. Heteronuclear decoupling was performed during data acquisition employing the SPINAL-64 decoupling sequence.

Enhancement factors for  $^{13}$ C were evaluated based on  $^{1}$ H  $\rightarrow$   $^{13}$ C cross-polarization (CP) MAS experiments. The contact time in these experiments was set to 2 ms; a ramped pulse was applied on the  $^{1}$ H-channel. 512 scans with a recycle delay of 4 s were recorded. Nominal values of the enhancement factors were obtained by scaling the peak maxima of the  $\mu$ w off spectra to those of the  $\mu$ w on spectra. The errors of the enhancement factors were estimated by adding the percentage error of the noise level of both acquired spectra. The corresponding spectra and enhancement factors are shown in Section S4 of the Supporting Information.

Saturation recovery experiments were employed to determine the polarization buildup of the investigated carbon atoms. These experiments were performed with microwave irradiation ( $\mu$ w on). A pulse train consisting of twenty  $\pi/2$ -pulses with a respective pulse length of 3.5  $\mu$ s and a spacing of 5 ms between the pulses was used to initially quench the <sup>13</sup>C magnetization. Buildup times  $\tau_b$  of 16, 32, 64, 128, 250, 500, and 1400 s were used, recording 64 scans for Triton and 32 scans for all other surfactant samples.

To selectively address the direct polarization transfer path, a pulse sequence introduced by the authors in an earlier publication was applied. <sup>40</sup> In this pulse sequence, the standard saturation recovery experiment was modified by the addition of a train of rotor-synchronized  $\pi$ -pulses with a pulse length of 6  $\mu$ s and a pulse spacing of 500 ms on the <sup>1</sup>H channel during the buildup of <sup>13</sup>C magnetization, which purges the buildup of <sup>1</sup>H magnetization.

The obtained spectra of the direct polarization pathway were subtracted from the spectra showing the superposition of the direct and indirect pathways to obtain the spectra only displaying the indirect polarization pathway. The spectra were deconvoluted using Lorentzian line shapes to determine intensities for all signals. The intensities of the signals of interests, namely the PEG units of the surfactants, were plotted against the utilized  $\tau_{\rm b}$  to allow for further analysis.

Additionally, exemplary heteronuclear correlation (HET-COR) experiments were conducted to verify the data obtained from the DNP NMR spectra and to confirm the model developed in this work. The data as well as the experimental details are shown in Section S7 of the Supporting Information.

#### 3. RESULTS AND DISCUSSION

**3.1.** Characterization of the Mesoporous Silica Materials. To characterize the utilized silica materials and in order to understand their pore structure, the materials were inspected by adsorption/desorption experiments utilizing the BET model for analysis. <sup>54</sup> Table 1 summarizes the results of these measurements.

Table 1. Characterization Results Obtained by the Adsorption/Desorption Measurements

| method/material                                 | SBA-15 | MCM 41 |
|---|--------|--------|
| BET surface area/m <sup>2</sup> g <sup>-1</sup> | 555    | 899    |
| pore size (NLDFT)/nm                            | 7.0    | 4.0    |
| pore volume (Gurvich)/cm³ g <sup>-1</sup>       | 0.76   | 0.89   |
| pore surface/m <sup>2</sup> g <sup>-1</sup>     | 534    | 1040   |

Unlike MCM 41, SBA-15 usually features micropores in the form of channels connecting the mesopores. <sup>61</sup> However, the contribution of these micropores to the total pore volume is small, <sup>62</sup> especially for SBA-15 materials with a moderate surface area, as the one utilized in this study. <sup>63</sup> Therefore, the micropores are not discussed further in this work. The pore size distribution obtained by NLDFT is shown in Figure S1 in the Supporting Information.

As the goal of this work was to probe a potential influence of confinement on the polarization transfer behavior of polarizing agents dissolved in surfactants, two different pore sizes were chosen for investigation. To achieve that, SBA-15 and MCM 41 mesoporous silica materials were used. In order to understand how the surfactants interact with the pore surface, it is integral to consider the size of these molecules in comparison to the size of the pore they are confined in. To evaluate whether the pores could accommodate the guest molecules, their maximum size is estimated based on their stretched conformation using a 3D modeling program, namely Chem3D. The amount of ethylene glycol units considered for the length estimation for each of the polydisperse surfactants is based on their composition analysis published previously.<sup>40</sup>

The shortest surfactant investigated in this work is PEG 200, with an average of four ethylene glycol units and an approximate length of 1.6 nm. The other estimated lengths are 1.9 nm for  $\rm E_5$ , 3.5 nm for  $\rm C_{10}\rm E_6$  and 4.1 nm for Triton. As interactions of the surfactants and the pore wall are certainly taking place, an at least partially perpendicular orientation of the surfactant molecules on the pore wall is assumed. Hence, the dimension of relevance for the adsorption of the surfactants into the pores is the pore diameter. A conceivable lengthwise adsorption along the pore axis is entropically unfavorable as it would not represent the structure with the largest cohesive force.  $^{64}$ 

A comparison of these estimated lengths to the pore diameters reveals that all surfactants can be accommodated by the SBA-15 material in an arbitrary orientation, even in their longest assumed conformation. As for the MCM 41 porous material, especially the larger surfactants investigated in this work,  $C_{10}E_6$  and Triton with an average of six and nine ethylene glycol units, respectively, are approximately as long or longer than the pore diameter. However, as the investigated surfactants are not rigid molecules, they are expected to coil via the formation of inter- and intramolecular hydrogen bonds for the PEG units and van der Waals interactions for the hydrocarbons, as well as by entropic forces. This behavior

reduces the effective length of the surfactants to a fraction of their length in the stretched conformation, <sup>69,70</sup> therefore allowing for the absorption into the pores.

For AMUPol, a size of 1.8 nm is estimated with its polyethylene chain fully stretched. Therefore, the polarizing agent is significantly smaller than the pores of the utilized silica materials, enabling the radical to be absorbed into the pores easily.

**3.2.** <sup>13</sup>C MAS DNP Spectra. Figure 2 shows the <sup>13</sup>C MAS ssNMR spectra obtained for the samples investigated in this study for a long buildup time of 1400 s where the signal-tonoise ratio is the highest and, thus, spectral features are best observable. In Figure 2, each column represents one of the surfactants, while each row corresponds to one of the two amorphous silica materials. The spectra for the direct and indirect pathway, their superposition as well as the spectra without microwave irradiation (with their respective magnification factors for better visibility, if applicable) are displayed.

PEG 200 and  $E_5$  only display two resonances for all recorded spectra. The signal at approximately 60 ppm corresponds to the carbon atoms at the end of the PEG chain, next to the terminal hydroxyl group. The signal at 70 ppm is attributed to all other carbon atoms in the PEG chain, as they are not discernible under the utilized experimental conditions.

For these two surfactants, the resonances assigned to the direct and indirect polarization transfer pathway are almost of the same size for the sample confined in SBA-15. Both signals are evenly enhanced through the direct polarization experiments for both sets of resonances. For the samples confined in MCM 41, the resonances assigned to the indirect polarization transfer pathway are predominant, leading to overall negative signals in the superposition of both polarization transfer pathways.

 $C_{10}E_6$  and Triton display additional signals to those caused by the PEG unit. As can be seen in Figure 1,  $C_{10}E_6$  contains an aliphatic decyl unit that causes signals between 0 and 40 ppm. However, these signals overlap severely so that only four distinct signals are discernible under the present conditions. For both utilized amorphous silica materials, the resonances assigned to the indirect polarization transfer pathway of those carbon atoms are larger than those for the direct polarization transfer pathway. As indirect polarization transfer is favored on certain nuclei based on their dynamics or their proximity to the polarizing agent, <sup>15,40,50</sup> this implies that these carbons take part in motional fluctuations with correlation times shorter than the inverse resonance frequency or that there is a large distance between them and the AMUPol molecules. <sup>71–73</sup> Aliphatic chains are lipophilic, therefore hindering interactions with the hydrophilic AMUPol. Hence, a larger indirect signal is expected here.

Triton features a tetramethylbutylphenyl moiety in addition to the PEG units, which causes signals between 0 and 40 ppm for the aliphatic carbons as well as between 105 and 160 ppm for the aromatic carbons (see Figure 1).

Due to their poor signal quality, the signals not corresponding to PEG units were not analyzed and discussed in this work.

To get more insights into the relation of the polarizing agent with the investigated confined surfactants, the signals attributed to the PEG units were deconvoluted, resulting in the signal intensities for the direct and indirect pathway, respectively. The signal intensity produced by direct polarization is expressed as percentage of the total signal intensity,

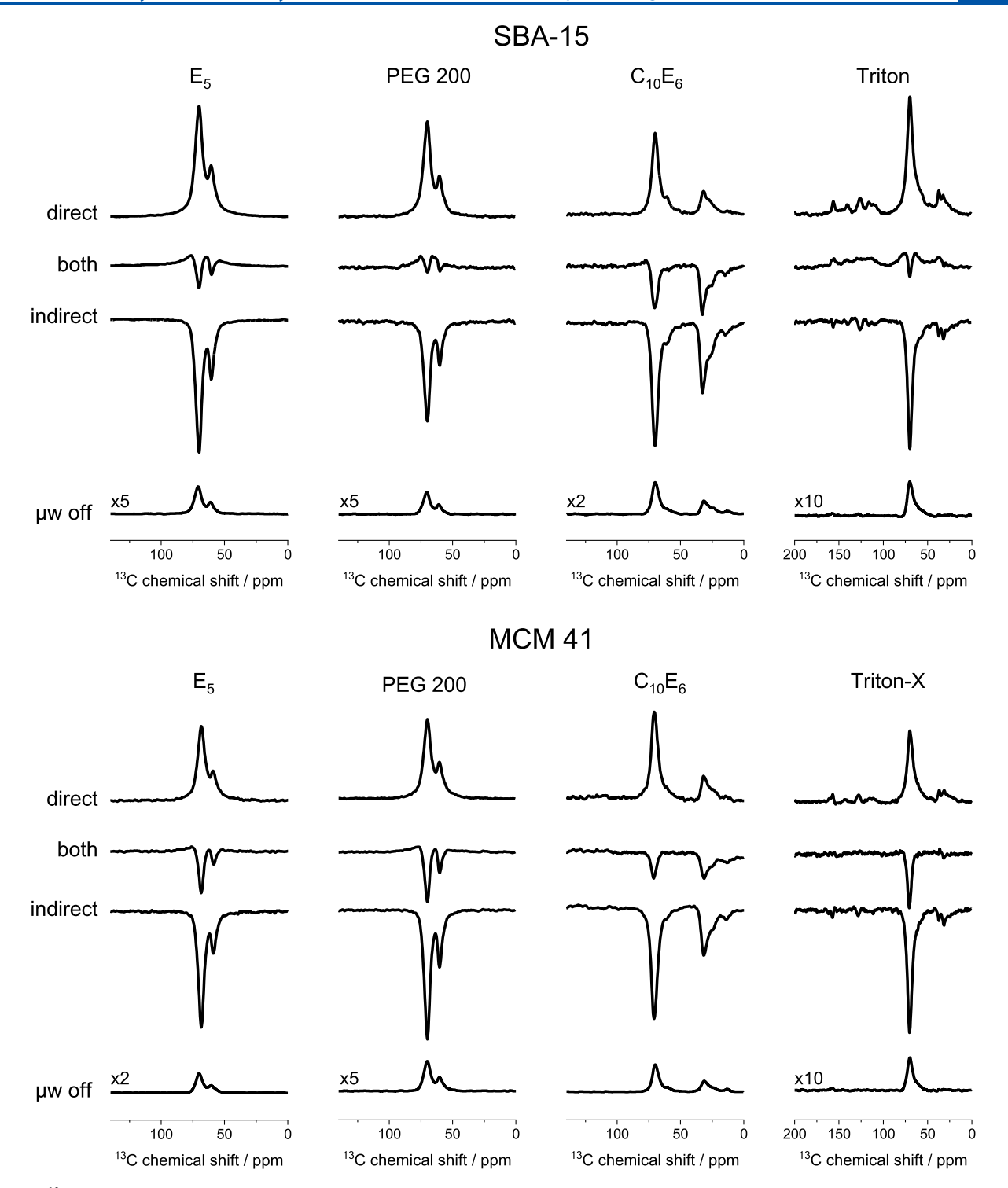


Figure 2.  $^{13}$ C MAS ssNMR spectra acquired in this work at a buildup time of 1400 s. The spectra obtained for the direct and indirect polarization as well as their superposition are displayed in the first three rows of spectra for each spectra set. Also shown are the spectra measured without  $\mu$ w irradiation with their respective scaling factors for better visibility. The upper panel shows the spectra obtained for SBA-15, and the lower panel shows the spectra obtained for MCM 41.

as established in our previous work. Figure 3 summarizes the obtained results for all investigated samples, allowing a comparison of the polarizing behavior of the different samples.

For  $E_5$  and for PEG 200, similar curves are observed in Figure 3. Both the carbons at the end of the PEG chain at 60 ppm as well as the carbons in the chain itself at 70 ppm display approximately 40–60% of direct polarization expressed as percentage of the total signal intensity. However, the silica

materials in which the surfactants are confined appear to have significant influence on the polarization transfer pathway. On average, the  $E_5$  and the PEG 200 confined in MCM 41 display less direct polarization transfer than those confined in SBA-15. This indicates the involvement of motions of the PEG units on a timescale shorter than the inverse resonance frequency or a larger spatial distance between the carbons of the surfactants confined in the MCM 41 as compared to those in the SBA-15

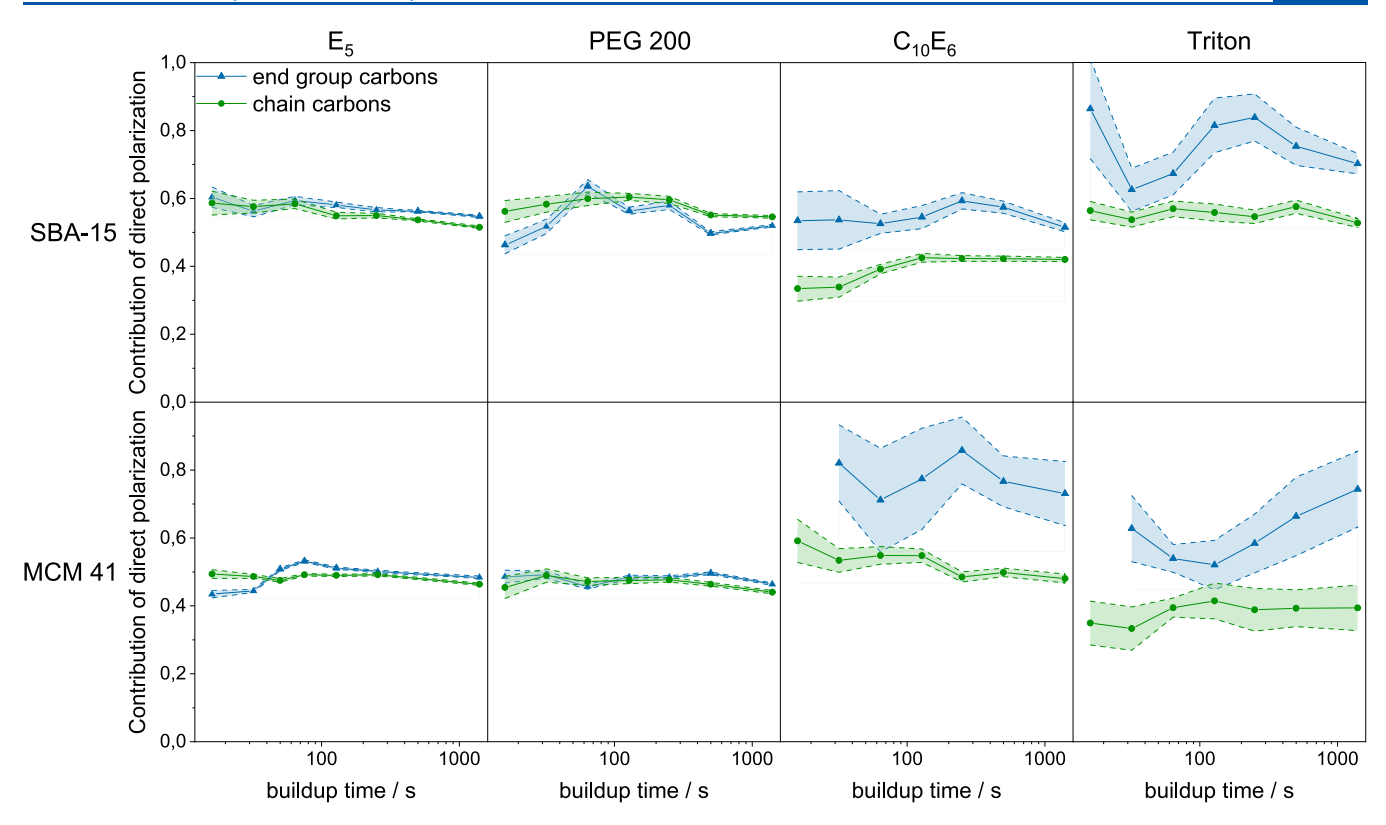


Figure 3. Ratios of signal intensity produced via direct polarization compared to the total signal intensity for the carbons of the PEG unit for all surfactants confined in the two mesoporous silica materials, SBA-15 and MCM 41.

.49,50 As discussed above, the AMUPol molecule is small enough to be confined into the pores of the mesoporous MCM 41. Therefore, it is unlikely that the smaller pore size leads to considerably higher distance between the carbon atoms of the surfactants and the polarizing agent. It is more likely that the smaller pore size increases the statistical disorder of the confined molecules, therefore impeding interactions between the molecules and allowing for higher mobility of the PEG chains.

For C<sub>10</sub>E<sub>6</sub> and Triton, differences between the carbons at the end of the PEG moieties and those in the middle of the chain become apparent. The carbons at the end show a significantly higher amount of direct polarization than the ones in the middle of the chain. This might seem counterintuitive, since a high mobility is expected for these carbons, as observed for bulk C<sub>10</sub>E<sub>6</sub> in an earlier report by some of the authors. <sup>41</sup> This high mobility would substantiate ideal conditions for the indirect polarization transfer pathway, assuming the time scale of the dynamics is different from the corresponding Larmor frequencies. 74,75 However, specific interactions with the amorphous silica material need to be considered as well. For E<sub>5</sub> and PEG 200, it is assumed that the majority of the carbon atoms interact with the silica materials in a similar manner since they have very similar properties in terms of hydrophilicity. Additionally, all carbons are neighboring oxygen atoms that are able to accept hydrogen bonds. Statistically, any carbon can point toward the silica surface and the terminal hydroxyl group could also point inward into the coiled PEG to form hydrogen bonds. The molecules C<sub>10</sub>E<sub>6</sub> and Triton consist of a hydrophilic moiety (the PEG unit) and a hydrophobic moiety (the aliphatic carbon chain and the tetramethylbutylphenyl group, respectively) and are amphiphilic. The hydrophobic groups cannot interact with the

surface of the silica pores and cannot form hydrogen bonds. It is, therefore, assumed that these moieties are oriented toward the pore center, leaving the PEG unit pointing toward the wall of the pore. Since AMUPol is a hydrophilic radical,<sup>51</sup> it is also assumed that it is concentrated primarily toward the pore wall where the PEG units of the amphiphilic surfactants are located. From the data presented in Figure 3, it is assumed that the terminal hydroxyl group of the amphiphilic surfactants is responsible for the main interactions with the surface of the silica pores as it shows a high amount of direct pathway polarization, indicating low mobility due to the strong hydrogen bonds and close proximity to the polarizing agent. The lipophilic part of the surfactants, which cannot fold onto the hydrophilic PEG units, points toward the pore center, away from the AMUPol, causing the observed larger amount of indirect channel polarization.

**3.3. Line Width Analysis.** To further illustrate the effect of the confinement on the surfactants as well as to confirm the results obtained by analyzing the contributions of the direct and indirect pathways, the full widths at half maximum (FWHM) of the signals are evaluated. The FWHM of the investigated signals for all samples at  $\tau_{\rm b} = 1400$  s are shown in Figure 4.

For all observed signals, the indirect pathway resonances display a smaller line width than the corresponding resonances assigned to the direct polarization pathway, as shown in Figure 4 and observed in Figure 2. This is in agreement with observations made in earlier works concerning similar surfactant systems. The signals of the indirect polarization pathway are caused by the transfer of polarization from the proton reservoir to the observed carbon nucleus. This allows for the observation of nuclei farther away from the polarizing agent, since the polarization can travel through the

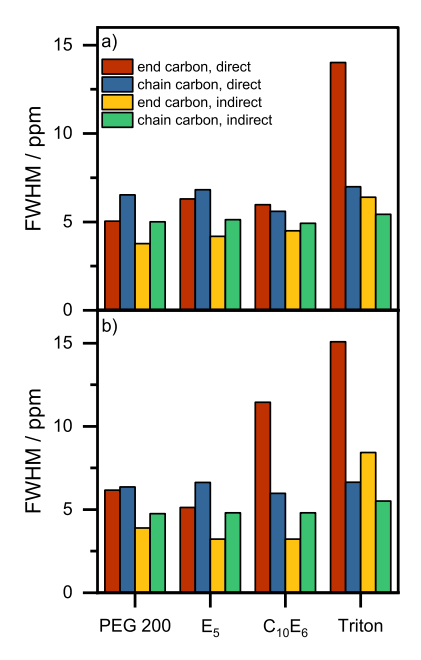


**Figure 4.** FWMH of the signals caused by direct polarization and those caused by indirect polarization corresponding to the end group and the chain carbons of the PEG units of all investigated surfactants confined in (a) SBA-15 and (b) MCM 41.

whole sample via the proton reservoir. Carbon atoms polarized by the direct polarization pathway need to be in direct contact with the radical moiety to be polarized. Hence, the carbons corresponding to the indirect signal do not experience the same amount of paramagnetic broadening, leading to narrower signals.

For  $E_5$  and PEG 200, the signals corresponding to the PEG chain are approximately as broad as or slightly broader than those corresponding to the end group carbons, indicating a similar proximity of the end group carbons and the chain carbons to the polarizing agent.

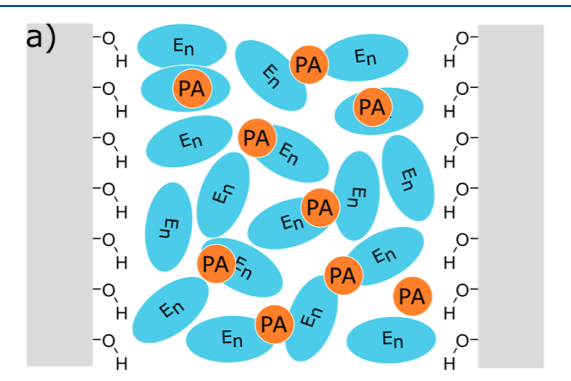
For the amphiphilic surfactants,  $C_{10}E_6$  and Triton, a different trend is observable. Despite the signal at 70 ppm corresponding to more nuclei that all experience a slightly different environment, the signal assigned to the direct polarization pathway that corresponds to the end groups is as broad (for the case of  $C_{10}E_6$  confined in SBA-15) or significantly broader than that of the ethylene glycol chain (for  $C_{10}E_6$  confined in MCM 41 and for all confined Triton

samples). Additionally, upon closer inspection of the spectra displayed in Figure 2, it is apparent that the end group carbons exhibit substantially less signal than those in the PEG units. As the end groups have been observed to display more direct than indirect polarization and are therefore more likely to be closer to the hydrophilic polarizing agent AMUPol, they are likely to experience large broadening due to the contact with the paramagnetic radical moiety, rendering the signal unobservable in the most severe cases. Unlike the chain carbons, there are no end group carbons facing away from the polarizing agent that could contribute to a narrow indirect polarization transfer pathway signal for Triton. Hence, the broadening translates into the observed indirect signals corresponding to the end group carbons, leading to unusually broad signals for the resonances assigned to the indirect polarization transfer pathway. This indicates that the polarizing agent highly localized at the end group carbons. For C<sub>10</sub>E<sub>6</sub>, a strong broadening of the indirect signal of the end group carbons is not observed, suggesting a slightly better mixing of the AMUPOL with the PEG units of the  $C_{10}E_6$ .

**3.4.** Development of a Model for the Surfactant Arrangement in the Pores. According to the data obtained by the line width analysis and the determination of the relative contribution of the direct and indirect polarization pathway, a schematic representation is developed to show the arrangement of the surfactant in the silica pores. The corresponding illustration can be found in Figure 5. Here, the silica walls are displayed in a stylized manner, with the surfactants being represented in two different arrangements, depending on whether they are hydro- or amphiphilic.

The hydrophilic surfactants,  $E_5$  and PEG 200, coil and mix with the hydrophilic polarizing agent AMUPol, forming a homogeneous mixture. Additionally, each carbon of the two investigated PEGs has an equal opportunity to be in close proximity to the silica wall, since each carbon neighbors an oxygen atom capable of forming hydrogen bonds. Therefore, no differences in polarization behavior or line width are observed for the end group carbon atoms compared to the chain carbon atoms.

For the amphiphilic surfactants,  $C_{10}E_6$  and Triton, it has been shown that the carbon atoms in the end group experience more direct polarization than those located in the PEG chains. To explain the larger amount of direct polarization experienced by the end groups, they have to be located in a close proximity to the polarizing agent, closer than the rest of the PEG chain carbons. The dominance of the direct polarization transfer



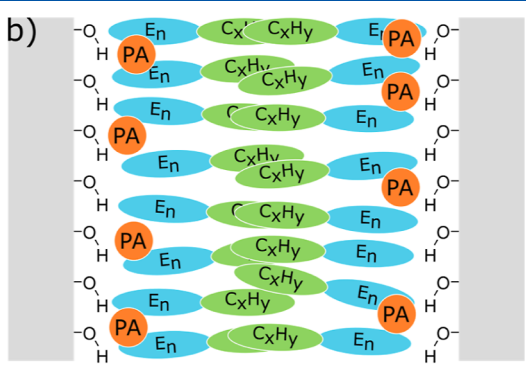


Figure 5. Schematic illustration of (a) the hydrophilic surfactants ( $E_5$  and PEG 200) and (b) the amphiphilic surfactants ( $C_{10}E_6$  and Triton) oriented in the pores of the mesoporous silica host material.  $E_n$  represents the PEG units,  $C_xH_y$  represents the lipophilic moiety of the amphiphilic surfactants and PA represents the polarizing agent AMUPol (not to scale).

pathway also indicates a lack of dynamics, indicating that the hydroxyl group at the end of the PEG unit mediates the interactions of the molecule with the silica walls, forming hydrogen bonds. In addition, the analysis of the FWHM has shown a large broadening of the signal of the end groups for both surfactants that is caused by the interactions of the carbons with a paramagnetic moiety, namely the radical centers of the polarizing agent. This further confirms the adjacency of the polarizing agent and the end group carbon atoms. Considering the present data, an arrangement of the amphiphilic surfactants as shown in Figure 5b is highly likely.

Interestingly, this work has shown that the influence of the pore size on the arrangement of the surfactants in the pore is negligible. Both systems, those with surfactants confined in SBA-15 as well as in MCM 41, show very similar patterns of polarization transfer and line widths.

## 4. CONCLUSIONS

DNP-enhanced ssNMR of two different classes of surfactants employing AMUPol as polarization agent was used to investigate how four commercially available surfactants ( $E_{\rm s}$ , PEG 200,  $C_{\rm 10}E_{\rm 6}$ , and Triton) interact with two different mesoporous silica materials, SBA-15 and MCM 41. DSC measurements were performed to confirm that the surfactants are indeed confined in the pores of the silica materials and to observe the changes in their melting and crystallization behavior while confined.

A previously established relative method was used to quantify the proportion of directly transferred polarization expressed as a percentage of the total signal intensity in order to achieve comparable results across all samples, independent of radical concentration and amount of sample used. Employing this method, it could be shown that each of the carbon atoms in PEG 200 and  $\rm E_{\rm S}$  interacts with the silica pore and the polarizing agent in a similar manner, leading to an even pattern of polarization transfer across all of them. Both the terminal carbon atom as well as the atoms in the PEG chain receive equal amounts of direct polarization.

For  $C_{10}E_6$  and Triton, the terminal carbon of the PEG chain receives more direct polarization than the ones in the chain, indicating that the terminal carbons are less mobile due to the interactions of the hydroxyl group with the wall of the silica pores. It also indicates a close proximity of the hydrophilic AMUPol with the PEG units of the surfactants.

Through the analysis of the signal line widths of the investigated signals, it could be shown that the signals corresponding to the end groups of the PEG chains are broader for the amphiphilic surfactants compared to those of the hydrophilic surfactants. This indicates a close spatial proximity of the radical moieties of the polarizing agent to the end group carbons, leading to paramagnetic broadening and bleaching of the signal.

Combining the data collected in this work, a model of the arrangement of the surfactants in the silica mesopores could be developed, illustrating that the hydrophilic surfactants interact with the pore surface in a significantly different manner than the amphiphilic ones.

This work illustrates that the method of measuring direct polarization DNP-enhanced ssNMR spectra aids in understanding the complex interplay of confined molecules with their host system. Especially, the combination of direct and indirect polarization with line width analyses allows for the development of a model of how different classes of surfactants

arrange themselves within the pores of their mesoporous silica host materials. It also extends the use of a relative method of spectral analysis of direct and indirect DNP NMR spectra, enabling the comparison of different samples without having to account for sample mass or the exact concentration of the polarizing agent.

# ASSOCIATED CONTENT

# **Supporting Information**

The Supporting Information is available free of charge at https://pubs.acs.org/doi/10.1021/acs.jpcc.3c01946.

Details on utilized chemicals including structural analysis detailing the lengths of the polydisperse surfactants; pore size distribution of the utilized SBA-15; DSC data and their interpretation;  $^{1}H \rightarrow ^{13}C$  CP MAS DNP NMR spectra and their interpretation; exemplary deconvolution of  $^{13}C$  DNP NMR spectra;  $^{13}C$  buildup curves; and exemplary HETCOR spectra (PDF)

#### AUTHOR INFORMATION

# **Corresponding Author**

Gerd Buntkowsky — Department of Chemistry, Eduard-Zintl-Institute for Inorganic and Physical Chemistry, Technical University of Darmstadt, 64287 Darmstadt, Germany;

orcid.org/0000-0003-1304-9762;

Email: gerd.buntkowsky@chemie.tu-darmstadt.de

#### **Authors**

Sonja C. Döller – Department of Chemistry, Eduard-Zintl-Institute for Inorganic and Physical Chemistry, Technical University of Darmstadt, 64287 Darmstadt, Germany

Martin Brodrecht – Department of Chemistry, Eduard-Zintl-Institute for Inorganic and Physical Chemistry, Technical University of Darmstadt, 64287 Darmstadt, Germany

Torsten Gutmann — Department of Chemistry, Eduard-Zintl-Institute for Inorganic and Physical Chemistry, Technical University of Darmstadt, 64287 Darmstadt, Germany; orcid.org/0000-0001-6214-2272

Markus Hoffmann — Department of Chemistry and Biochemistry, State University of New York College at Brockport, Brockport, New York 14420, United States; orcid.org/0000-0002-5469-8665

Complete contact information is available at: https://pubs.acs.org/10.1021/acs.jpcc.3c01946

#### Notes

The authors declare no competing financial interest.

### ACKNOWLEDGMENTS

Financial support by the Deutsche Forschungsgemeinschaft under Contract Bu-911-24-2 and by the National Science Foundation under grant no. 1953428 are gratefully acknowledged. We thank Rochester Midland Corporation for donating the polydisperse surfactants.

#### REFERENCES

- (1) François, I.; Sandra, K.; Sandra, P. Comprehensive Liquid Chromatography: Fundamental Aspects and Practical Considerations—A Review. *Anal. Chim. Acta* **2009**, *641*, 14–31.
- (2) Li, Z.; Rösler, L.; Wissel, T.; Breitzke, H.; Gutmann, T.; Buntkowsky, G. Immobilization of a Chiral Dirhodium Catalyst on SBA-15 via Click-Chemistry: Application in the Asymmetric Cyclo-

- propanation of 3-Diazooxindole With Aryl Alkenes. J. CO2 Util. 2021, 52, 101682–101690.
- (3) Costa, J. A. S.; de Jesus, R. A.; Santos, D. O.; Neris, J. B.; Figueiredo, R. T.; Paranhos, C. M. Synthesis, Functionalization, and Environmental Application of Silica-Based Mesoporous Materials of the M41S and SBA-n Families: A Review. *J. Environ. Chem. Eng.* **2021**, *9*, 105259–105288.
- (4) Murillo-Cremaes, N.; López-Periago, A. M.; Saurina, J.; Roig, A.; Domingo, C. Nanostructured Silica-Based Drug Delivery Vehicles for Hydrophobic and Moisture Sensitive Drugs. *J. Supercrit. Fluids* **2013**, 73, 34–42
- (5) Brodrecht, M.; Kumari, B.; Thankamony, A. S. S. L.; Breitzke, H.; Gutmann, T.; Buntkowsky, G. Structural Insights into Peptides Bound to the Surface of Silica Nanopores. *Chem.—Eur. J.* **2019**, 25, 5214–5221.
- (6) Brodrecht, M.; Kumari, B.; Breitzke, H.; Gutmann, T.; Buntkowsky, G. Chemically Modified Silica Materials as Model Systems for the Characterization of Water-Surface Interactions. *Z. Phys. Chem.* **2018**, 232, 1127–1146.
- (7) Zhao, D.; Feng, J.; Huo, Q.; Melosh, N.; Fredrickson, G. H.; Chmelka, B. F.; Stucky, G. D. Triblock Copolymer Syntheses of Mesoporous Silica with Periodic 50 to 300 Angstrom Pores. *Science* **1998**, 279, 548–552.
- (8) Beck, J. S.; Vartuli, J. C.; Roth, W. J.; Leonowicz, M. E.; Kresge, C. T.; Schmitt, K. D.; Chu, C. T. W.; Olson, D. H.; Sheppard, E. W.; McCullen, S. B.; et al. A New Family of Mesoporous Molecular Sieves Prepared with Liquid Crystal Templates. *J. Am. Chem. Soc.* **1992**, *114*, 10834–10843.
- (9) Kumari, B.; Brodrecht, M.; Breitzke, H.; Werner, M.; Grünberg, B.; Limbach, H.-H.; Forg, S.; Sanjon, E. P.; Drossel, B.; Gutmann, T.; et al. Mixtures of Alcohols and Water confined in Mesoporous Silica: A Combined Solid-State NMR and Molecular Dynamics Simulation Study. J. Phys. Chem. C 2018, 122, 19540–19550.
- (10) Ben Shir, I.; Kababya, S.; Schmidt, A. Binding Specificity of Amino Acids to Amorphous Silica Surfaces: Solid-State NMR of Glycine on SBA-15. *J. Phys. Chem. C* **2012**, *116*, 9691–9702.
- (11) Dosseh, G.; Xia, Y.; Alba-Simionesco, C. Cyclohexane and Benzene Confined in MCM-41 and SBA-15: Confinement Effects on Freezing and Melting. *J. Phys. Chem. B* **2003**, *107*, 6445–6453.
- (12) Alba-Simionesco, C.; Coasne, B.; Dosseh, G.; Dudziak, G.; Gubbins, K. E.; Radhakrishnan, R.; Sliwinska-Bartkowiak, M. Effects of Confinement on Freezing and Melting. *J. Phys.: Condens. Matter* **2006**, *18*, R15–R68.
- (13) Gedat, E.; Schreiber, A.; Albrecht, J.; Emmler, T.; Shenderovich, I.; Findenegg, G. H.; Limbach, H.-H.; Buntkowsky, G. <sup>2</sup>H-Solid-State NMR Study of Benzene-d<sub>6</sub> Confined in Mesoporous Silica SBA-15. *J. Phys. Chem. B* **2002**, *106*, 1977–1984.
- (14) Hassan, J. Analysis of 2H NMR Spectra of Water Molecules on the Surface of Nano-Silica Material MCM-41: Deconvolution of the Signal Into a Lorentzian and a Powder Pattern Line Shapes. *Phys. B* **2012**, *407*, 179–183.
- (15) Buntkowsky, G.; Döller, S. C.; Haro-Mares, N.; Gutmann, T.; Hoffmann, M. Solid-State NMR Studies of Non-Ionic Surfactants Confined in Mesoporous Silica. Z. Phys. Chem. **2022**, 236, 939–960.
- (16) Amitay-Rosen, T.; Kababya, S.; Vega, S. A Dynamic Magic Angle Spinning NMR Study of the Local Mobility of Alanine in an Aqueous Environment at the Inner Surface of Mesoporous Materials. *J. Phys. Chem. B* **2009**, *113*, 6267–6282.
- (17) Amitay-Rosen, T.; Vega, S. A Deuterium MAS NMR Study of the Local Mobility of Dissolved Methionine and Di-Alanine at the Inner Surface of SBA-15. *Phys. Chem. Chem. Phys.* **2010**, *12*, 6763–6773.
- (18) Werner, M.; Rothermel, N.; Breitzke, H.; Gutmann, T.; Buntkowsky, G. Recent Advances in Solid State NMR of Small Molecules in Confinement. *Isr. I. Chem.* **2014**. *54*. 60–73.
- (19) Buntkowsky, G.; Breitzke, H.; Adamczyk, A.; Roelofs, F.; Emmler, T.; Gedat, E.; Grünberg, B.; Xu, Y.; Limbach, H.-H.; Shenderovich, I.; et al. Structural and Dynamical Properties of Guest

- Molecules Confined in Mesoporous Silica Materials Revealed by NMR. *Phys. Chem. Chem. Phys.* **2007**, *9*, 4843–4853.
- (20) Anastas, P. T.; Warner, J. C. Green Chemistry: Theory and Practice; Oxford University Press: Oxford, 1998.
- (21) Hoffmann, M. M. Polyethylene Glycol as a Green Chemical Solvent. Curr. Opin. Colloid Interface Sci. 2022, 57, 101537.
- (22) La Sorella, G.; Strukul, G.; Scarso, A. Recent Advances in Catalysis in Micellar Media. *Green Chem.* **2015**, *17*, 644–683.
- (23) Fernandez, A. M.; Held, U.; Willing, A.; Breuer, W. H. New Green Surfactants for Emulsion Polymerization. *Prog. Org. Coat.* **2005**, *53*, 246–255.
- (24) Andrade, C. Z.; Alves, L. Environmentally Benign Solvents in Organic Synthesis: Current Topics. *Curr. Org. Chem.* **2005**, *9*, 195–218
- (25) de Oliveira, C. A. F.; Guimares, C. R. W.; de Alencastro, R. B. Molecular Dynamics Study on Liquid 1-Octanol. *Int. J. Quantum Chem.* **2000**, *80*, 999–1006.
- (26) Huyskens, P.; Ruelle, P. Dynamic Equilibrium Time Fractions or Fractional Lifetimes? The Final Chapter. *J. Mol. Liq.* **2000**, *88*, 87–108
- (27) Hu, K.; Zhou, Y.; Shen, J.; Ji, Z.; Cheng, G. Microheterogeneous Structure of 1-Octanol in Neat and Water-Saturated State. *J. Phys. Chem. B* **2007**, *111*, 10160–10165.
- (28) Döller, S. C.; Brodrecht, M.; Haro Mares, N. B.; Breitzke, H.; Gutmann, T.; Hoffmann, M.; Buntkowsky, G. Deuterium NMR Studies of the Solid–Liquid Phase Transition of Octanol-d<sub>17</sub> Confined in SBA-15. *J. Phys. Chem. C* **2021**, *125*, 25155–25164.
- (29) Zaera, F. Probing Liquid/Solid Interfaces at the Molecular Level. Chem. Rev. 2012, 112, 2920–2986.
- (30) Blum, F. D.; Xu, G.; Liang, M.; Wade, C. G. Dynamics of Poly(vinyl acetate) in Bulk and on Silica. *Macromolecules* **1996**, *29*, 8740–8745.
- (31) Buntkowsky, G.; Vogel, M. Small Molecules, Non-Covalent Interactions, and Confinement. *Molecules* **2020**, 25, 3311–3342.
- (32) Rorschach, H.; Hazlewood, C. Protein Dynamics and the NMR Relaxation Time  $T_1$  of Water in Biological Systems. *J. Magn. Reson.* **1986**, 70, 79–88.
- (33) Brown, M. F.; Ribeiro, A. A.; Williams, G. D. New View of Lipid Bilayer Dynamics from <sup>2</sup>H and <sup>13</sup>C NMR Relaxation Time Measurements. *Proc. Natl. Acad. Sci. U.S.A.* **1983**, *80*, 4325–4329.
- (34) Weigler, M.; Winter, E.; Kresse, B.; Brodrecht, M.; Buntkowsky, G.; Vogel, M. Static Field Gradient NMR Studies of Water Diffusion in Mesoporous Silica. *Phys. Chem. Chem. Phys.* **2020**, 22, 13989–13998.
- (35) Ni, Q. Z.; Daviso, E.; Can, T. V.; Markhasin, E.; Jawla, S. K.; Swager, T. M.; Temkin, R. J.; Herzfeld, J.; Griffin, R. G. High Frequency Dynamic Nuclear Polarization. *Acc. Chem. Res.* **2013**, *46*, 1933–1941.
- (36) Griffin, R. G.; Prisner, T. F. High Field Dynamic Nuclear Polarization—The Renaissance. *Phys. Chem. Chem. Phys.* **2010**, *12*, 5737—5740.
- (37) Lesage, A.; Lelli, M.; Gajan, D.; Caporini, M. A.; Vitzthum, V.; Miéville, P.; Alauzun, J.; Roussey, A.; Thieuleux, C.; Mehdi, A.; et al. Surface Enhanced NMR Spectroscopy by Dynamic Nuclear Polarization. *J. Am. Chem. Soc.* **2010**, *132*, 15459–15461.
- (38) Daube, D.; Aladin, V.; Heiliger, J.; Wittmann, J. J.; Barthelmes, D.; Bengs, C.; Schwalbe, H.; Corzilius, B. Heteronuclear Cross-Relaxation under Solid-State Dynamic Nuclear Polarization. *J. Am. Chem. Soc.* **2016**, *138*, 16572–16575.
- (39) Bothe, S.; Hoffmann, M. M.; Gutmann, T.; Buntkowsky, G. Comparative Study of the Magnetic Field Dependent Signal Enhancement in Solid-State Dynamic Nuclear Polarization Experiments. J. Phys. Chem. C 2017, 121, 27089–27097.
- (40) Hoffmann, M. M.; Bothe, S.; Gutmann, T.; Hartmann, F.-F.; Reggelin, M.; Buntkowsky, G. Directly vs. Indirectly Enhanced <sup>13</sup>C in Dynamic Nuclear Polarization Magic Angle Spinning NMR Experiments of Nonionic Surfactant Systems. *J. Phys. Chem. C* **2017**, 121, 2418–2427.

- (41) Hoffmann, M. M.; Bothe, S.; Gutmann, T.; Buntkowsky, G. Unusual Local Molecular Motions in the Solid State Detected by Dynamic Nuclear Polarization Enhanced NMR Spectroscopy. *J. Phys. Chem. C* **2017**, *121*, 22948–22957.
- (42) Aladin, V.; Corzilius, B. Methyl Dynamics in Amino Acids Modulate Heteronuclear Cross Relaxation in the Solid State Under MAS DNP. *Solid State Nucl. Magn. Reson.* **2019**, *99*, 27–35.
- (43) Aladin, V.; Vogel, M.; Binder, R.; Burghardt, I.; Suess, B.; Corzilius, B. Complex Formation of the Tetracycline-Binding Aptamer Investigated by Specific Cross-Relaxation under DNP. *Angew. Chem., Int. Ed.* **2019**, *58*, 4863–4868.
- (44) Ni, Q. Z.; Markhasin, E.; Can, T. V.; Corzilius, B.; Tan, K. O.; Barnes, A. B.; Daviso, E.; Su, Y.; Herzfeld, J.; Griffin, R. G. Peptide and Protein Dynamics and Low-Temperature/DNP Magic Angle Spinning NMR. *J. Phys. Chem. B* **2017**, *121*, 4997–5006.
- (45) Park, H.; Uluca-Yazgi, B.; Heumann, S.; Schlögl, R.; Granwehr, J.; Heise, H.; Schleker, P. P. M. Heteronuclear Cross-Relaxation Effect Modulated by the Dynamics of N-Functional Groups in the Solid State Under <sup>15</sup>N DP-MAS DNP. *J. Magn. Reson.* **2020**, 312, 106688–106694
- (46) Biedenbänder, T.; Aladin, V.; Saeidpour, S.; Corzilius, B. Dynamic Nuclear Polarization for Sensitivity Enhancement in Biomolecular Solid-State NMR. *Chem. Rev.* **2022**, *122*, 9738–9794.
- (47) Aladin, V.; Sreemantula, A. K.; Biedenbänder, T.; Marchanka, A.; Corzilius, B. Specific Signal Enhancement on an RNA-Protein Interface by Dynamic Nuclear Polarization. *Chem.—Eur. J.* **2023**, 29, e202203443—e202203454.
- (48) Biedenbänder, T.; de Jesus, V.; Schmidt-Dengler, M.; Helm, M.; Corzilius, B.; Fürtig, B. RNA Modifications Stabilize the Tertiary Structure of tRNAfMet by Locally Increasing Conformational Dynamics. *Nucleic Acids Res.* **2022**, *50*, 2334–2349.
- (49) Döller, S. C.; Gutmann, T.; Hoffmann, M.; Buntkowsky, G. A Case Study on the Influence of Hydrophilicity on the Signal Enhancement by Dynamic Nuclear Polarization. *Solid State Nucl. Magn. Reson.* **2022**, *122*, 101829–101837.
- (50) Hoffmann, M. M.; Bothe, S.; Brodrecht, M.; Klimavicius, V.; Haro-Mares, N. B.; Gutmann, T.; Buntkowsky, G. Direct and Indirect Dynamic Nuclear Polarization Transfer Observed in Mesoporous Materials Impregnated with Nonionic Surfactant Solutions of Polar Polarizing Agents. J. Phys. Chem. C 2020, 124, 5145–5156.
- (51) Sauvée, C.; Rosay, M.; Casano, G.; Aussenac, F.; Weber, R. T.; Ouari, O.; Tordo, P. Highly Efficient, Water-Soluble Polarizing Agents for Dynamic Nuclear Polarization at High Frequency. *Angew. Chem., Int. Ed.* **2013**, *52*, 10858–10861.
- (52) Brodrecht, M.; Breitzke, H.; Gutmann, T.; Buntkowsky, G. Biofunctionalization of Nano Channels by Direct In-Pore Solid-Phase Peptide Synthesis. *Chem.—Eur. J.* **2018**, *24*, 17814–17822.
- (53) Wang, X.; Lin, K. S. K.; Chan, J. C. C.; Cheng, S. Direct Synthesis and Catalytic Applications of Ordered Large Pore Aminopropyl-Functionalized SBA-15 Mesoporous Materials. *J. Phys. Chem. B* **2005**, *109*, 1763–1769.
- (54) Brunauer, S.; Emmett, P. H.; Teller, E. Adsorption of Gases in Multimolecular Layers. *J. Am. Chem. Soc.* **1938**, *60*, 309–319.
- (55) Klyachko-Gurvich, A. L. An Improved Method of Determining Surface Area by the Adsorption of Air. Russ. Chem. Bull. 1961, 10, 1756–1758.
- (56) Barrett, E. P.; Joyner, L. G.; Halenda, P. P. The Determination of Pore Volume and Area Distributions in Porous Substances. I. Computations from Nitrogen Isotherms. *J. Am. Chem. Soc.* **1951**, *73*, 373–380.
- (57) Ravikovitch, P. I.; Haller, G. L.; Neimark, A. V. Density Functional Theory Model for Calculating Pore Size Distributions: Pore Structure of Nanoporous Catalysts. *Adv. Colloid Interface Sci.* **1998**, 76–77, 203–226.
- (58) Schneider, S.; Säckel, C.; Brodrecht, M.; Breitzke, H.; Buntkowsky, G.; Vogel, M. NMR Studies on the Influence of Silica Confinements on Local and Diffusive Dynamics in LiCl Aqueous Solutions Approaching their Glass Transitions. *J. Chem. Phys.* **2020**, 153, 244501–244513.

- (59) Kirschenbaum, L. J.; Riesz, P. Sonochemical Degradation of Cyclic Nitroxides in Aqueous Solution. *Ultrason. Sonochem.* **2012**, *19*, 1114–1119.
- (60) Fung, B. M.; Khitrin, A. K.; Ermolaev, K. An Improved Broadband Decoupling Sequence for Liquid Crystals and Solids. *J. Magn. Reson.* **2000**, *142*, 97–101.
- (61) Kruk, M.; Jaroniec, M.; Ko, C. H.; Ryoo, R. Characterization of the Porous Structure of SBA-15. *Chem. Mater.* **2000**, *12*, 1961–1968.
- (62) Janus, R.; Wądrzyk, M.; Lewandowski, M.; Natkański, P.; Łątka, P.; Kuśtrowski, P. Understanding Porous Structure of SBA-15 upon Pseudomorphic Transformation into MCM-41: Non-Direct Investigation by Carbon Replication. *J. Ind. Eng. Chem.* **2020**, 92, 131–144.
- (63) Matos, J. R.; Mercuri, L. P.; Kruk, M.; Jaroniec, M. Toward the Synthesis of Extra-Large-Pore MCM-41 Analogues. *Chem. Mater.* **2001**, *13*, 1726–1731.
- (64) Drach, M.; Narkiewicz-Michałek, J.; Rudziński, W.; Findenegg, G. H.; Király, Z. Calorimetric Study of Adsorption of Non-Ionic Surfactants on Silica Gels: Estimating the Role of Lateral Interactions Between Surface Aggregates. *Phys. Chem. Chem. Phys.* **2002**, *4*, 2307–2319.
- (65) Hoffmann, M. M.; Too, M. D.; Paddock, N. A.; Horstmann, R.; Kloth, S.; Vogel, M.; Buntkowsky, G. On the Behavior of the Ethylene Glycol Components of Polydisperse Polyethylene Glycol PEG 200. *J. Phys. Chem. B* **2023**, *127*, 1178–1196.
- (66) Kawai, S.; Foster, A. S.; Björkman, T.; Nowakowska, S.; Björk, J.; Canova, F. F.; Gade, L. H.; Jung, T. A.; Meyer, E. Van der Waals Interactions and the Limits of Isolated Atom Models at Interfaces. *Nat. Commun.* **2016**, *7*, 11559–11565.
- (67) Margenau, H. Van der Waals Forces. Rev. Mod. Phys. 1939, 11, 1–35.
- (68) Schauperl, M.; Podewitz, M.; Waldner, B. J.; Liedl, K. R. Enthalpic and Entropic Contributions to Hydrophobicity. *J. Chem. Theory Comput.* **2016**, *12*, 4600–4610.
- (69) Dohmen, M. P. J.; Pereira, A. M.; Timmer, J. M. K.; Benes, N. E.; Keurentjes, J. T. F. Hydrodynamic Radii of Polyethylene Glycols in Different Solvents Determined from Viscosity Measurements. *J. Chem. Eng. Data* **2008**, *53*, 63–65.
- (70) Linegar, K. L.; Adeniran, A. E.; Kostko, A. F.; Anisimov, M. A. Hydrodynamic Radius of Polyethylene Glycol in Solution Obtained by Dynamic Light Scattering. *Colloid J.* **2010**, *72*, 279–281.
- (71) Macdonald, P. M.; Soong, R. The Truncated Driven NOE and <sup>13</sup>C NMR Sensitivity Enhancement in Magnetically-Aligned Bicelles. *J. Magn. Reson.* **2007**, *188*, 1–9.
- (72) Mao, J.; Aladin, V.; Jin, X.; Leeder, A. J.; Brown, L. J.; Brown, R. C. D.; He, X.; Corzilius, B.; Glaubitz, C. Exploring Protein Structures by DNP-Enhanced Methyl Solid-State NMR Spectroscopy. *J. Am. Chem. Soc.* **2019**, *141*, 19888–19901.
- (73) Lilly Thankamony, A. S.; Wittmann, J. J.; Kaushik, M.; Corzilius, B. Dynamic Nuclear Polarization for Sensitivity Enhancement in Modern Solid-State NMR. *Prog. Nucl. Magn. Reson. Spectrosc.* **2017**, *102–103*, 120–195.
- (74) Luo, X.-L.; Howard, J. A. K.; Crabtree, R. H. <sup>1</sup>H NMR T<sub>1</sub>(min) Data and Structure in a Series of Rhenium Polyhydride Complexes and the Contribution of M-H Dipole-Dipole Relaxation. *Org. Magn. Reson.* **1991**, 29, S89–S93.
- (75) Jarymowycz, V. A.; Stone, M. J. Fast Time Scale Dynamics of Protein Backbones: NMR Relaxation Methods, Applications, and Functional Consequences. *Chem. Rev.* **2006**, *106*, 1624–1671.